Additive Manufacturing of Polyamide 6/66 Copolymer Nanocomposites: Thermal and Flammability Properties

Steven D. Kim[1,2], Abdullah Kafi[3], Hao Wu[2], Stuart Bateman[3], Joseph H. Koo[1,2]*

[1]Department of Mechanical Engineering, The University of Texas at Austin, Austin, TX 78712, USA

[3]KAI, LLC, Austin, TX 78739, USA

[2]School of Engineering, RMIT University, Melbourne, VIC 3000, Australia

*jkoo@mail.utexas.edu

ABSTRACT

As one of the most commonly used methods of additive manufacturing (AM), fused filament fabrication (FFF) has drawn a great amount of interest in both industry and academia. The purpose of this study is to develop a flame retardant (FR) polyamide 6/polyamide 66 (PA6/66) nanocomposite with reduced flammability and enhanced thermal and mechanical properties, while simultaneously maintaining the printability for commercially available FFF machines. In this study, varying amounts of FR, thermoplastic elastomer (K), nanoclay (NC), and multiwall carbon nanotubes (MWNT) were melt compounded via twin-screw extrusion to prepare PA6/66 nanocomposite pellets. The flame retardant and thermal properties of these formulations were characterized using microscale combustion calorimeter (MCC) and thermogravimetric analysis (TGA). Based on MCC, it was found that formulations 2, 4, and 5 yielded best results, while formulation 3 and 2 gave best results in TGA testing. Finally, three FR PA6/66 formulations (2, 4, and 5) were down-selected, 3D printed via FFF, and used for flammability, thermal, and mechanical properties characterizations. Due to difficulties in 3D printing, only formulation 5 was successfully printed and tested. However, despite not being the best performing formulation, formulation 5 yielded promising results in UL 94 and tensile tests. Lastly, Micro-CT analysis displayed that formulation 5 was much more porous in comparison to the neat PA6/66 system.

1. INTRODUCTION

Additive manufacturing is a method of production in which products are produced by building the object layer by layer. While many unique AM technologies, such as fused filament fabrication (FFF), stereolithography apparatus (SLA), and selective laser sintering (SLS) all offer methods for rapid prototyping, FFF is more widely used for its ease of use and low cost. Due to this rapid rise in AM technologies, it is important to develop new and improved 3D printable high-performance materials. However, there are not many papers published in the literature studying FFF compatible flame retardant materials.

Although FFF was developed in the 1980s, it is more widely known today as fused deposition modeling or FDM. FFF creates parts by feeding a filament that is often 1.75 mm in diameter through a heated extruder head which moves in the X and Y axes. This extruder head then deposits the molten material onto a heated build platform in a predetermined pattern. Once a layer is complete, the build platform is lowered by a specific layer height distance, and the extruder begins to deposit the material for the following layer. This process is repeated until the final product is complete. Due to its greatly improved user interface, low cost, and versatility, FFF is the preferred method for use in this experiment.

Polyamide 6/polyamide 66 copolymer is a thermoplastic polymer developed to improve the existing properties found in polyamide 6 and polyamide 66. PA6/66 offers varying desirable properties, such as good chemical resistance, great impact strength, and low density. Despite the various advantages, PA6/66, like other polyamides, readily absorbs moisture which in turn can hinder the processability and printability of the copolymer. Since PA6/66 is derived from polyamide 6 and polyamide 66, its physical properties do not vastly differ; the density and melting temperature of PA6/66 are slightly lower than those of PA66.

Neat PA6/66 is inherently not flame retardant as per UL 94 test rating. When compounded with intumescent FR additives, the flammability properties are expected to drastically improve. Although adding greater amounts of flame retardant (FR) additive results in greater flammability results, this also results in weaker mechanical properties as there is a lesser amount of PA6/66 remaining. Aside from the FR additive, some other additives were used in compounding PA6/66 formulations; these include, thermoplastic elastomer, nanoclay, and multiwall carbon nanotubes [1-5]. Adding specific amounts of nanomaterials is often attributed to enhancing various material properties, such as thermal, electrical, mechanical, or thermal. However, adding too much of a single additive can have adverse effects. Although polyamides are compatible with varying nanomaterial additives, the compatibility between the nanomaterials and between nanomaterial and polymer must be considered before compounding. Incompatibility between any of the materials or polymer and poor dispersion of nanomaterials can results in poor material properties.

In our previous study, it was found that FR will decompose when exposed to a flame, creating a protective char, thus protecting the material below it. However, as mentioned above, adding excessive FR may deteriorate mechanical properties. NC and MWNT are expected to improve the heat deflection temperature (HDT) of the polymer and help form a more solid char layer around the material. With the addition of just small amounts, such as 2.5 wt.% to 5 wt.% in the composite, NC and MWNT both exhibited significant increase in mechanical and FR performance [2, 6, 11-12]. Although both NC and MWNT show improved properties, increased loading exceeding 5 wt.% often leads to deterioration in mechanical properties, causing the polymer to become very brittle [1, 6-10]. Therefore, to combat the onset of brittleness, a thermoplastic elastomer K, which improves the elongation at break, will be added to restore the mechanical properties that are lost from FR, NC, and MWNT.

The objective of this research is to prepare an FFF compatible polyamide 6/polyamide 66 copolymer nanocomposite that exhibits improved flammability and mechanical properties since there is currently a lack of commercially available FR PA6/66 filaments. Although flammability properties will be improved with the addition of multiple components, it is also vital to maintain adequate levels of mechanical properties by adding an elastomer (K) component. To achieve this purpose, PA6/66 were blended with multiple additives consisting of FR, K, NC, and MWNT.

2. EXPERIMENTATION

2.1 Material and Processing

The pelletized PA6/66 was acquired from Zig Sheng Industrial Co. Ltd. and was used as the base material in the composite matrix. The FR and elastomer were provided by Clariant and Kraton, respectively. The NC was received from BYK and the MWNT was provided by Arkema as the last two additives.

PA6/66 was dried at 70°C for 24 hours before the compounding and extrusion process. As shown in Table 1, the FR varies from 15 wt.% to 10 wt.%. Although 15 wt.% FR loading is very likely to result in UL 94 V-0 rating, achieving this rating with just 10 wt.% FR loading would be preferred in order to retain more of the PA6/66 mechanical properties. Varying the wt.% of K from 10wt.% to 15wt.% will allow analysis for any significant changes to the elongation at break for the varying formulations. Lastly, the slight variation in the wt.% of NC and MWNT will allow analysis for any significant differences in mechanical properties. The following nine formulations (also denoted as F#) have been melt-compounded with the twin-screw extruder. Initial thermal and flammability properties on all nine formulations were tested via MCC and TGA. After initial analysis, three best performing formulations were down-selected for 3D printing and further analyzed for flammability and mechanical properties.

Table 1. PA6/66 Formulation Matrix

Formulation #	Formulation	PA 6/66 (wt.%)	FR (wt.%)	K (wt.%)	NC (wt.%)	MWNT (wt.%)
0	PA 6/66	100	-	-	-	-
1	15FR_10K_2.5NC_2.5MWNT	70	15	10	2.5	2.5
2	15FR_15K_2.5NC_2.5MWNT	65	15	15	2.5	2.5
3	15FR_10K_3.5NC_3.5MWNT	68	15	10	3.5	3.5
4	15FR_15K_3.5NC_3.5MWNT	63	15	15	3.5	3.5
5	10FR_10K_2.5NC_2.5MWNT	75	10	10	2.5	2.5
6	10FR_15K_2.5NC_2.5MWNT	70	10	15	2.5	2.5
7	10FR_10K_3.5NC_3.5MWNT	73	10	10	3.5	3.5
8	10FR_15K_3.5NC_3.5MWNT	68	10	15	3.5	3.5

In order to compound and process the PA6/66 formulations, a twin-screw extruder (Figure 1) was used. The Thermo Scientific Inc. Process 11 parallel twin-screw extruder serves to melt, mix, and

extrude FFF compatible filament. The entire twin-screw extruder setup consists of formulation feeder, heating chamber, motorized roller, and motorized spool. The mixed compound is first poured into the formulation feeder and the heating chamber, which consists of eight heating zones with temperatures varying from 230°C to 270°C, melts the compound and thoroughly mixes the polymer and additives into a filament. The twin screws that run along the length of the heating chamber is rotated at 150 rpm for optimal speed and quality of the filament. The extruded filament is then pulled by the motorized roller at a constant speed to ensure constant filament diameter. The motorized spool which rotates at approximately the same speed as the motorized roller then collects the filament into a spool for ease of transport. The extruded filaments are then used to conduct thermal characterization.

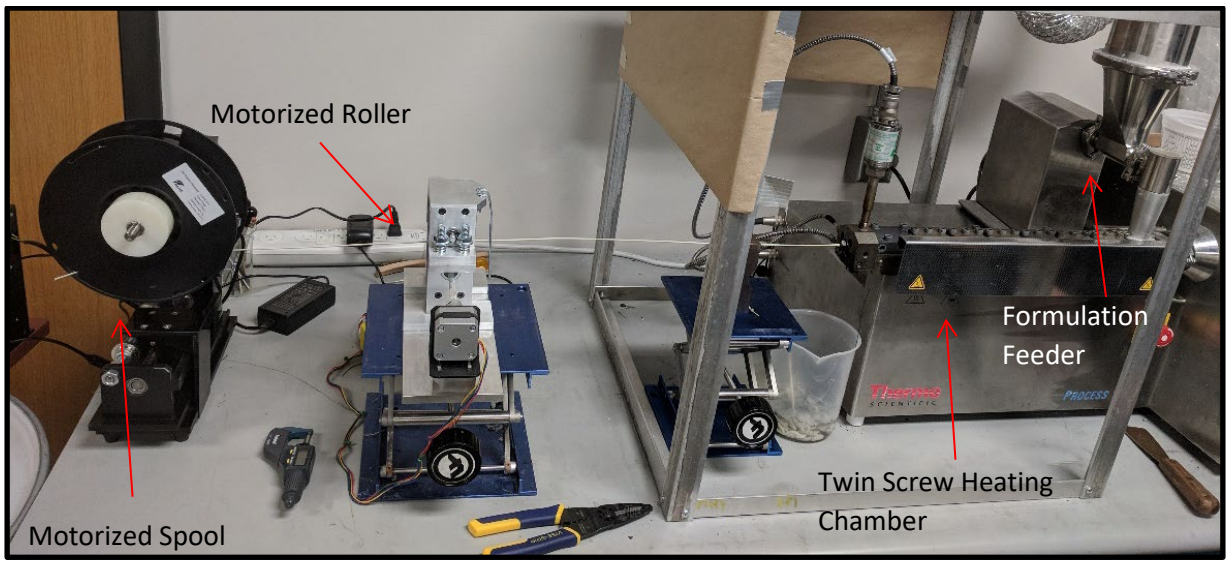

Figure 1. Image of twin-screw extruder setup.

2.2 Thermal Characterization

2.2.1 Microscale Combustion Calorimetry

Microscale Combustion Calorimetry (MCC) manufactured by Govmark Inc. was used to analyze heat release properties to predict flammability properties of each formulation. MCC utilizes approximately 2 to 3 mg of the formulation sample to conduct the analysis. The sample is loaded onto the ceramic rod showing in Figure 2 which is raised into the combustion chamber. The combustion chamber is held at constant 900°C while the pyrolyzer chamber is gradually heated from 100°C to 750°C at a rate of 1°C/s. The testing environment is controlled to be 80% nitrogen and 20% oxygen. This nitrogen and oxygen gas mixture is pumped through a tube containing desiccant to remove all moisture from the gas to ensure accurate results. MCC analyzes the oxygen levels in the testing chamber to provide heat release (HR) capacity, peak heat release rate (HRR), and total HR as a function of temperature. Each sample was tested in three non-repeated trials in accordance to ASTM D7309 standards.

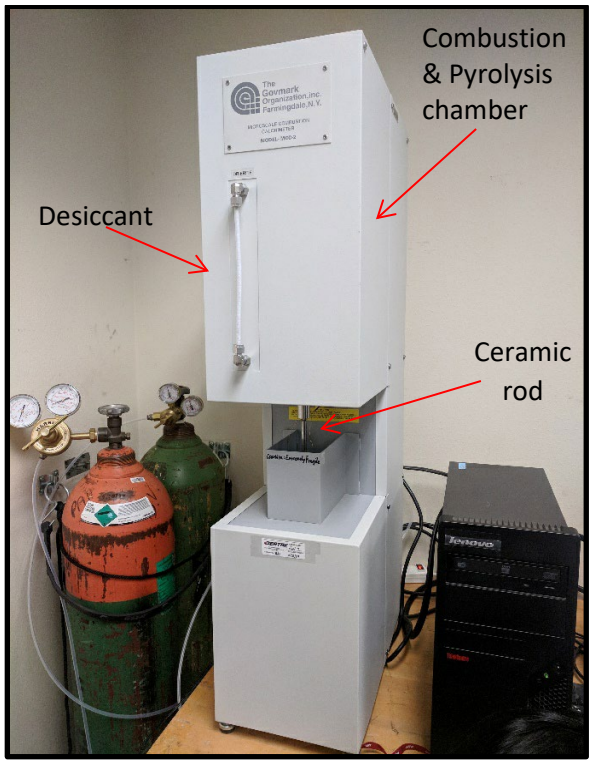

Figure 2. Image of Microscale Combustion Calorimetry instrument.

2.2.2 Thermogravimetric Analysis

After the completion of MCC analysis, thermogravimetric analysis (TGA) of all formulations was performed using TGA-50 developed by Shimadzu Scientific Instruments (Figure 3). Approximately 17 to 18 mg of the sample will be loaded into the heating chamber and heated to 1,000°C at a rate of 20°C/min in a nitrogen testing environment to measure the char yield as a function of temperature. Each sample will be analyzed once, then the six best performing formulations will be down-selected to be analyzed once again in the second trial. Then lastly, the top four best performing formulations will be analyzed for the third time in the third trial. After conducting the third TGA trial, data collected from MCC and TGA will be analyzed to select top three best performing formulations which will then be extruded using the twin-screw extruder at constant filament diameter of 1.75 ± 0.09 mm.

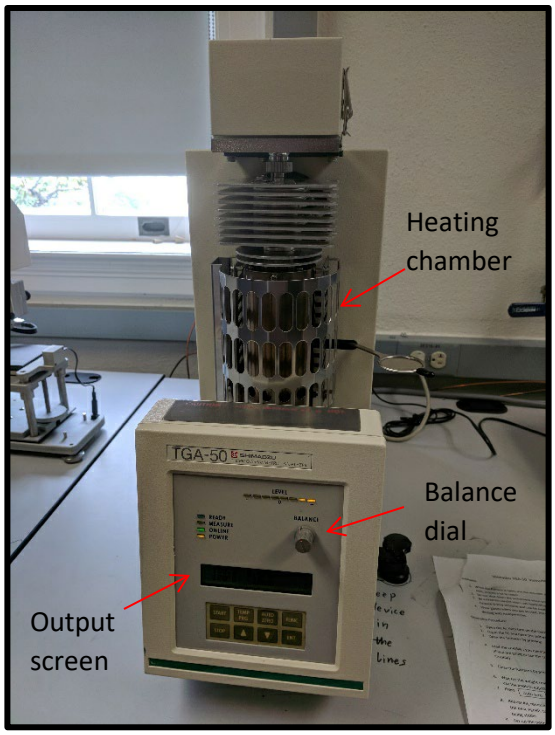

Figure 3. Image of Thermogravimetric Analysis instrument.

1.1 FFF Additive Manufacturing

After thorough data analysis of MCC and TGA results, a Craftunique CraftBot XL 3D printer was used to print five UL 94 and five tensile test bars (Figure 4) for each of the top three down-selected formulations. Same number of neat PA6/66 test bars will also be printed for control. The UL 94 test samples were 125mm long, 13mm wide, and 3mm thick. The tensile test specimens were 115mm long, 19mm wide, and 3mm thick. Additionally, the narrow sections of the tensile specimen were 33mm long and 6mm wide. The build platform will be maintained at 60°C and extruder head temperature of 260°C. The samples will be printed in a +45°/-45° raster infill pattern at 100% infill and a layer height of 0.1 mm. The printing speed will be limited to 60 mm/s.

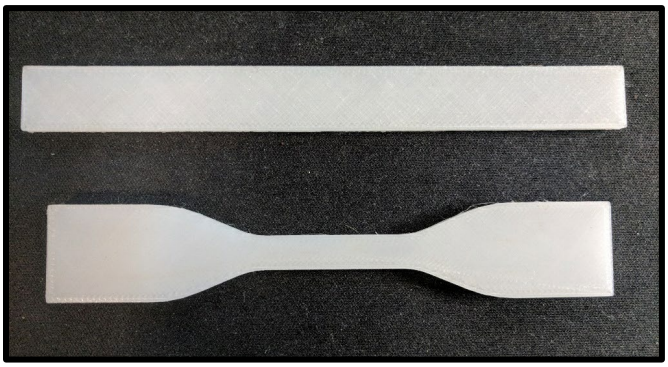

Figure 4. Image of FFF printed neat PA 6/66 test bars.

1.2 UL 94 Flammability Test

UL 94, which is a standardized thermoplastics flammability test used to analyze the safety of ablated plastics, was used after 3D printing UL 94 test models of the top three best performing formulations. The vertical UL 94 test ablates the test bar from the bottom using a flame at a 45-degree angle from the vertical test bar. The gas supply of the flame is timed such that after ten seconds of open flame, the gas supply shuts off automatically. Then, the first time (t1) is recorded until the test bar self-extinguishes. As soon as the test bar is fully extinguished, the flame is activated again for another ten seconds; the self-extinguishing time is once again measured as t2 and time for the after-glow to dissipate as t3. During the ablating and timing process, the test bar is also observed to determine if the test article melts and any dripping occurs. Using the three times and observation for dripping, the formulations are then rated as V-0, V-1, V-2, from best to worst. The specific rating criteria for UL 94 is shown in Table 2.

Table 2. UL 94 Rating Criteria

Criteria	V-0	V-1	V-2
Afterflame for each individual specimen (t1 and t2)	≤ 10s	≤ 30s	≤ 30s
Total afterflame for any condition set (t1+t2 for the 5 specimens)	≤ 50s	≤ 250s	≤ 250s
Afterflame plus afterglow time for each individual specimen after the second flame application	≤ 30s	≤ 60s	≤ 60s
Afterflame or afterglow of any specimen up to the holding clamp	No	No	No
Cotton indicator ignition	No	No	Yes

1.3 Tensile Test

In accordance with ASTM D638 type IV, an Instron Tension Tester 5966 was used to analyze the mechanical properties, such as tensile strength, modulus, and elongation at break, of each 3D printed tensile test bar. A crosshead type extensometer will be used to grip the test bars and then tested at room temperature with crosshead speed of 5 mm/min. With five tensile test bars for each of the top three down-selected formulations, each formulation will be tensile tested five times for better accuracy.

1.4 Micro-CT

First, the samples were scanned on a Bruker Skyscan 1275 operating at 40 kV 100 µA with no filter in place. The sample was placed on a brass stage and positioned to achieve an image pixel size. The height was adjusted to capture the thickest part of the sample. Samples were scanned with the following settings: 0.4° rotation step, 360° scanning, 4 frame averaging, total of 901 shadow projections (raw images). Camera settings were: 1944x1536 resolution, 67 ms exposure.

Second, a program, NRecon, is used to calculate cross sections from the raw images. With the software, post processing corrections were adjusted; corrections included smoothing, misalignment compensation, ring artifacts reduction, and beam-hardening correction (constant at

30% across all samples). The dynamic image range was set from 0.0 to 0.0170 for all samples. In order to analyze the volume inside the object, a rectangular shape ROI was set. The ROI (red rectangle) was created over a 2D slice and applied to all slices. Each slice was checked to make sure the ROI stays within the object. Adjustments to the ROI was made when necessary. Figure 5 below shows an image from the NRecon software window.

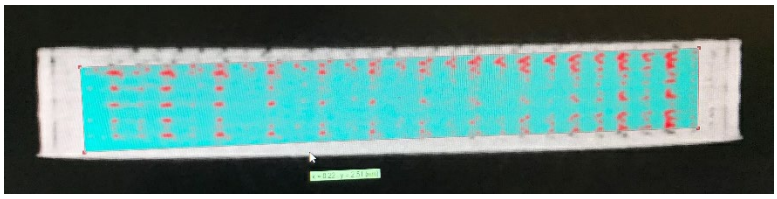

Figure 5. Snapshot from NRecon software showing raw data and reconstructed slice.

Analysis of the images were done using a CTan software. This software is used to binarize images in order to segregate areas of different density. Cross sections are represented as a binary image of material (1) and air (0). Porosity is calculated from the binarized images. Binarized images were exported as a model file and made into videos in CTVol.

2. RESULTS

2.1 MCC Results

MCC results shown in Table 3 display the average values from the three trials, the standard deviation, and the percentage improvement in comparison to the neat system (Formulation 0). The collected data indicate that formulations 2, 3, 4, and 5 had the best results.

Table 3. PA 6/66 MCC Data

	HR Capacity (J/g-K)		Peak HRR (W/g)		Total HR (kJ/g)	
Formulation	**Avg**	**StDev**	**Avg**	**StDev**	**Avg**	**StDev**
0	1301	39.6	1295	39.6	63.07	2.3
1	1022	181.9	1017	180.9	60.57	4.4
2	819	42.5	814	42.7	59.50	4.3
3	851	62.6	840	58.7	59.00	4.4
4	829	18.8	823	17.1	57.67	0.7
5	830	80.6	826	80.5	53.93	5.2
6	1060	102.8	1054	101.7	64.50	6.6
7	870	107.6	865	108.3	54.20	6.6
8	900	7.9	895	7.4	56.93	1.5

Figure 6 displays the average HR capacity of the formulation data acquired from MCC. When compared to the neat system, all formulations showed enhanced properties; of those formulations, F2 had the best results, closely followed by F4 and F5.

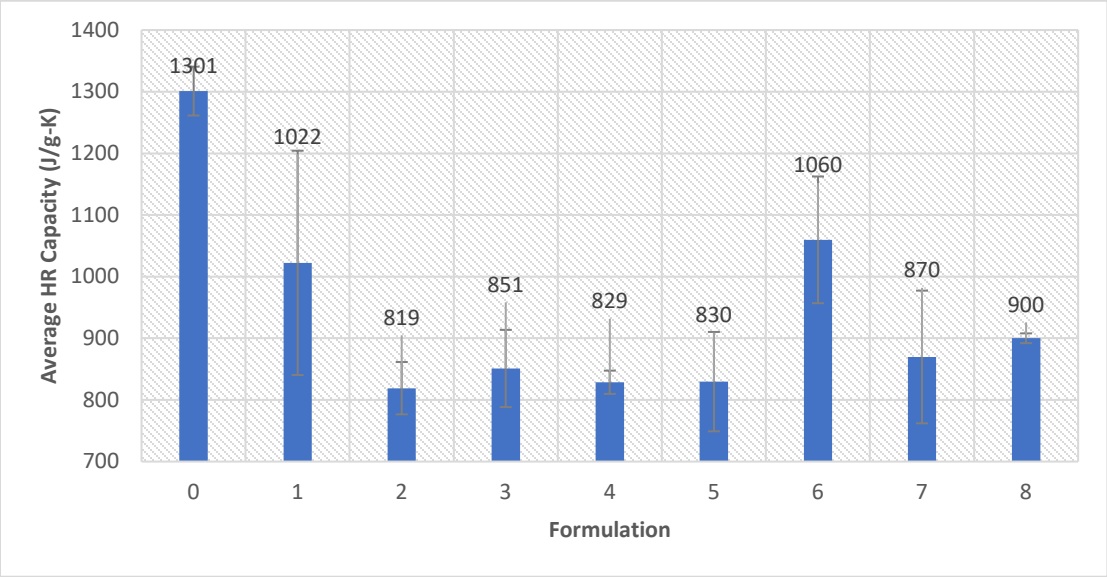

Figure 6. Graph of average HR Capacity of PA6/66 nanocomposites.

2.2 TGA Results

The averaged results from TGA are shown in Table 4, which include the temperatures at 10% mass loss, 50% mass loss, as well as temperatures at greatest mass loss (Max DrTGA). The main differences are shown in the temperatures at 10% mass loss. F1 through F4 all experienced 10% mass loss, on average, at 424°C, whereas F5 through F8 experienced it, on average, at a slightly higher temperature of 427°C. This factor can largely be attributed to F1~F4 having 15 wt.% FR while the subsequent formulations have only 12.5 wt.% FR. This result shows that having greater amounts of FR in a formulation causes the FR to decompose at a lower temperature, which forms the protective char layer earlier.

Table 4. PA6/66 TGA Data

	10% Mass Loss (°C)		50% Mass Loss (°C)		Max DrTGA (°C)	
Formulation	**Avg**	**StDev**	**Avg**	**StDev**	**Avg**	**StDev**
0	432	6.99	468	9.94	476	16.12
1	424	1.74	470	1.07	477	0.94
2	424	0.71	466	0.26	462	5.79
3	424	1.30	464	0.85	458	4.97
4	424	0.85	467	0.72	470	1.29
5	426	0.40	466	0.36	469	1.06
6	428	0.39	468	0.50	471	2.07
7	427	0.53	468	0.51	473	0.50
8	427	0.50	469	0.77	473	3.25

Figure 7 shows the TGA degradation curves of all nine formulations. All formulations begin at 100% weight but begins to deteriorate at a certain temperature. In the middle of the curve, the neat PA6/66 system lost its weight percentage noticeably faster than other formulations. This indicates that the additives used in all other formulations successfully improved the properties of PA6/66 by enhancing its thermal stability.

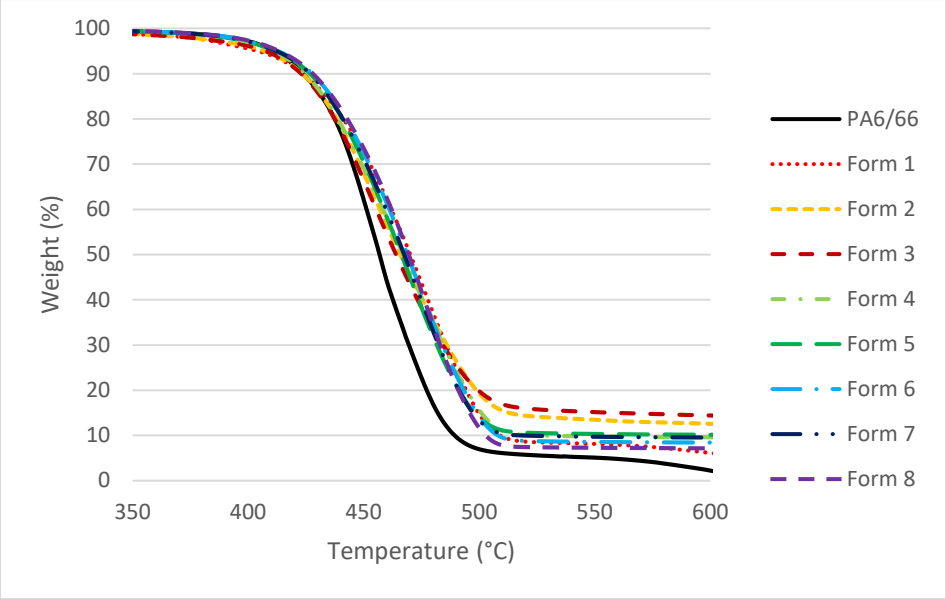

Figure 7. Degradation curves for all formulations (TGA, scan rate 20°C/min in N_2).

In observing the ends of the degradation curves, it is seen that F3 yielded the highest weight percentage, closely followed by F2. It is also important to note that all formulations performed better than the neat PA6/66 system by retaining more of its weight percentage after degradation.

Figure 8 shows the DrTGA curves for all formulations. As previously mentioned, DrTGA indicates at which temperature the greatest amount of mass loss occurred as well as the greatest amount of mass loss. Figure 8 indicates that all formulations either had a peak DrTGA value at a higher temperature or had lower peak mass loss values than the neat PA6/66 system. Furthermore, despite reaching the peak mass loss temperature earlier than other formulations, F1 through F4 display noticeably lower peak DrTGA than F5 through F8. This indicates that a lower peak mass loss temperature was caused by the additional FR, but this FR also assisted in lowering the peak mass loss value.

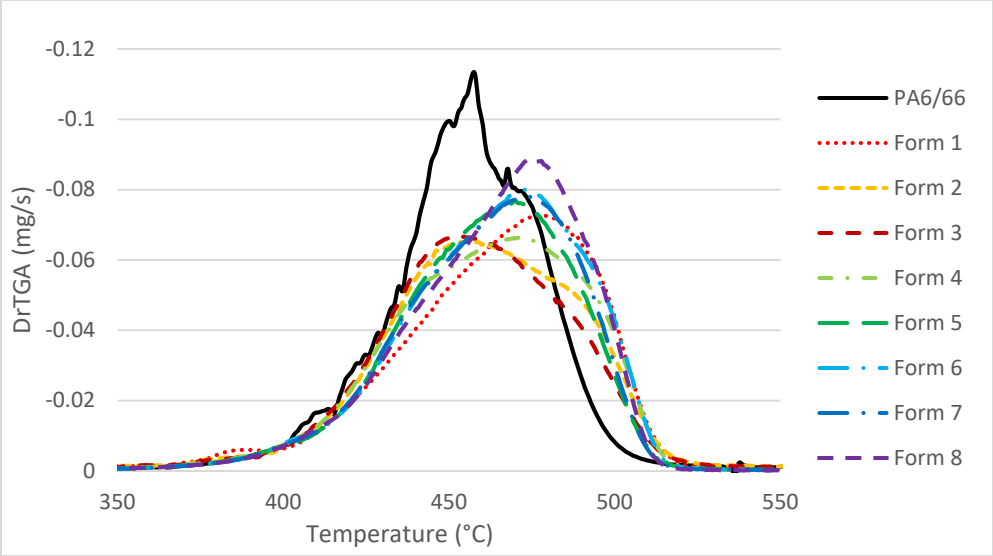

Figure 8. Peak derivative TGA curves for PA6/66 nanocomposites.

Upon analyzing the overall TGA data, it is seen that formulations F1 through F4, which had a higher weight percentage of FR at 15 wt.%, performed better than the subsequent formulations. However, the values between the formulations containing 15 wt.% and 12.5 wt.% FR were very similar. Also, the testing environment of TGA was 100% nitrogen gas, whereas the testing environment of MCC was 80% nitrogen and 20% oxygen gas, which more closely resembles real life atmospheric conditions. Therefore, the MCC data are weighted more heavily in the final decision-making to move forward with 3D printing and further testing. Taking these factors into consideration, the experiment moved forward with formulations 2, 4, and 5 to 3D print and perform further testing since these three formulations were the top performers in MCC and showed promising values in TGA.

2.3 FFF Printing

After close inspection of both MCC and TGA data, formulations 2, 4, and 5 were chosen as the top three down-selected formulations to attempt 3D printing with. These three were chosen because TGA results did not greatly vary between the formulations and F2, F4, and F5 displayed the best MCC results. In preparation for 3D printing, the top three formulations were extruded using the previously mentioned twin-screw extruder (Figure 1). Each of the three formulations were twice extruded to ensure good dispersion of the additives. When attempting to 3D print, however, it was found that F2 and F4 could not be printed on the CraftBot XL. It is speculated that this is due to the high concentration of additives that may be clogging the 0.4mm extruder nozzle. Although F2 and F4 could not be printed, F5 fortunately printed without any complications. After printing five test samples of tensile and UL 94 each for F5, the same amount was printed using the neat PA6/66 system as control. An image of the 3D printed UL 94 samples is shown in Figure 9.

Figure 9. Image of FFF printed F5 UL 94 test samples.

2.4 UL 94 Flammability Test Results

Due to previously mentioned difficulties in printing F2 and F4, UL 94 and tensile testing was only performed on F5. Table 5 shows the results from five UL 94 trials conducted on F5. The obtained results were not very consistent, which could be caused by a multitude of factors, from exact placement of the test specimen to accuracy of the timer used by the operator and the dispersion of FR within the polymer matrix. However, based on the retrieved data, it was concluded that this formulation did not achieve the UL 94 V-0 rating due to t2 being greater than the V-0 criteria of 10s.

Table 5. UL 94 Test Results of F5

PA 6/66 Formulation 5			
Sample #	t1 (s)	t2 (s)	Drip
1	1.8	57.6	No
2	0.5	1.7	No
3	1.7	113.8	No
4	0.6	58.9	No
5	0.0	15.1	No

Although the initial UL 94 test did not provide consistent t1 and t2 results, the test sample did not have any drips on all five trials. Furthermore, none of the five trials showed any afterglow after initial ablation. Therefore, it is likely that if the printing difficulties of F2 and F4 are resolved, these two formulations will show better results than F5 since F2 and F4 contain higher weight percentage of FR than F5. Figure 7 below shows an image of the UL 94 test samples after testing. Although two out of 5 samples warped due to the heat from the flame, none of the five samples experienced any heavy deformities, such as dripping.

Figure 10. Image of post-test F5 UL 94 test samples.

2.5 Tensile Testing

Tensile testing was only performed on the neat PA6/66 and F5. Table 6 shows the overall data collected from the neat PA6/66 tensile test (F0). These data are immediately followed by Table 7, which showcases tensile test data of F5 with comparison to F0.

Table 6. Tensile test results of Neat PA6/66 (F0)

Neat PA6/66			
Sample ID	**Ultimate Tensile Strength (MPa)**	**Modulus (MPa)**	**Elongation at Break (%)**
1	32.50	225.67	116.66
2	40.89	186.75	196.46
3	31.99	161.71	134.46
4	48.15	212.20	215.28
5	37.67	189.60	153.82
Std. Dev.	6.66	24.71	26.99
Avg.	38.24	195.19	163.33

Table 7. Tensile test results of PA6/66 F5 with % improvement from F0

Sample ID	Ultimate Tensile Strength (MPa)	Modulus (MPa)	Elongation at Break (%)
1	24.75	178.74	62.17
2	26.45	193.77	63.09
3	26.04	99.45	92.71
4	25.00	93.14	81.44
5	24.72	81.70	96.32
Std. Dev.	0.80	52.60	16.05
Avg.	25.39	129.36	79.15
% Improvement	-32%	-34%	-49%

As shown in Table 7, the average tensile strength of F5 was 25.39 MPa, which is 32% lower than F0. Although the tensile strength degraded, it was to be expected since multiple additives were added to each formulation. The modulus and elongation at break both show similar trends; modulus degraded by 34% while elongation at break degraded by 49%. Despite the deterioration of these values, it was as expected. Figure 11 below shows the stress vs. strain curve of both neat PA6/66 and F5. This figure further showcases the degraded mechanical properties of F5 when compared to the neat system. The enhanced flammability properties of F5 outweigh the decline of mechanical properties.

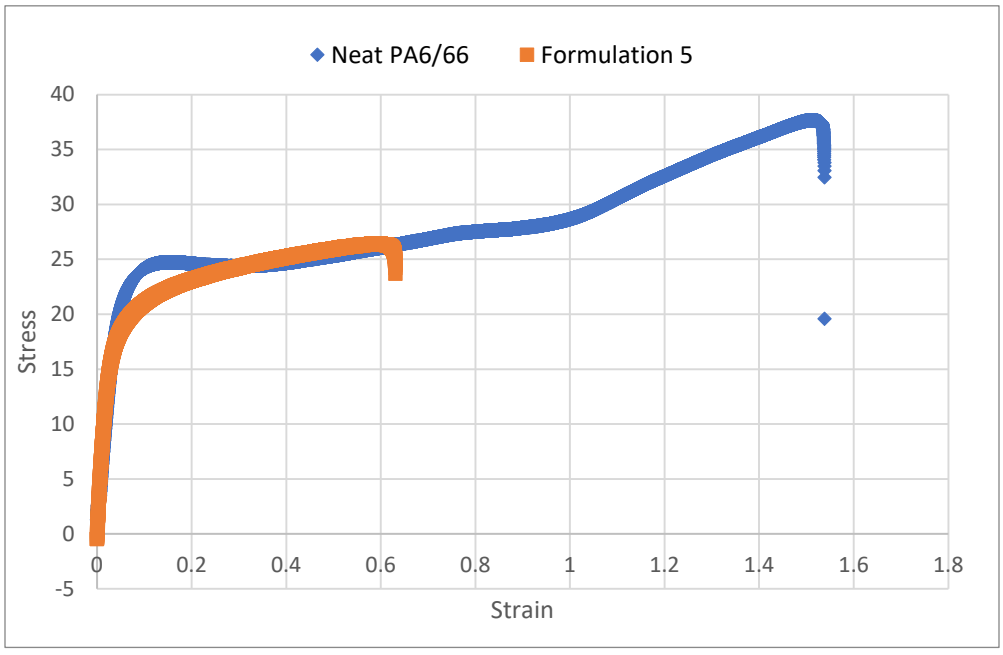

Figure 11. Stress vs. Strain curve of neat PA6/66 (F0) and F5.

2.6 Micro-CT Analysis

The total porosity is calculated as the volume of open and closed pores. Open pores are classified as the property of the volume of interest (VOI) as they intersect the boundary of VOI. A 'closed pore' in contrast a group of black pixels that is fully surrounded by a border of white pixels. Subsequently, closed pores are classified as a property of the material itself. Table 8 shows all porosity values are significantly lower for PA666 control (F0) than F5.

Table 8. Porosity results of PA6/66 samples (F0 and F5)

Properties	PA666 F0 (Control)	PA6/66 F5
Open Porosity, %	0.015	7.80
Closed Porosity, %	0.107	0.20
Total Pore Volume, mm^3	1.286	75.15
Total Porosity, %	0.121	7.99

F0 contains less pores and has a uniform distribution of pores localized around the center of tensile bar as shown in Figure 12. On the other hand, 3D models obtained from F5 showed porosity distributed throughout the surface of the sample. Results are in conformity with tensile properties as reported in Table 7.

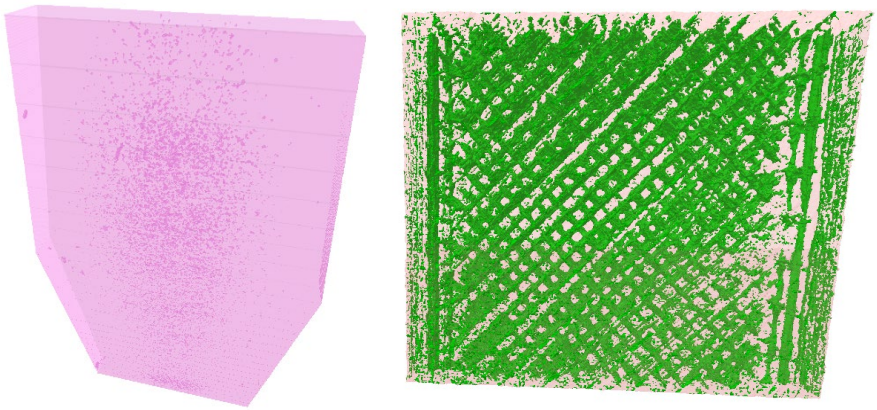

Figure 12. 3D models obtained from F0 (left) and F5 (right).

Micro-CT images of F0 (Figure 13) and F5 (Figure 14) further show differences in porosity between the two samples. Row b of both figures show the reconstructed model of F0 and F5. In comparing the two samples, F5 has visibly larger and greater number of pores within its cross-section. It is plausible that the greater porosity of F5 is due to the additives within the nanocomposite. These additives may have decreased the flow rate of the filament in the 3D printing process, resulting in less material extruding out of the printer nozzle. This decrease in material extruding from the nozzle may have resulted in the creation of pores and cavities in the 3D printed samples.

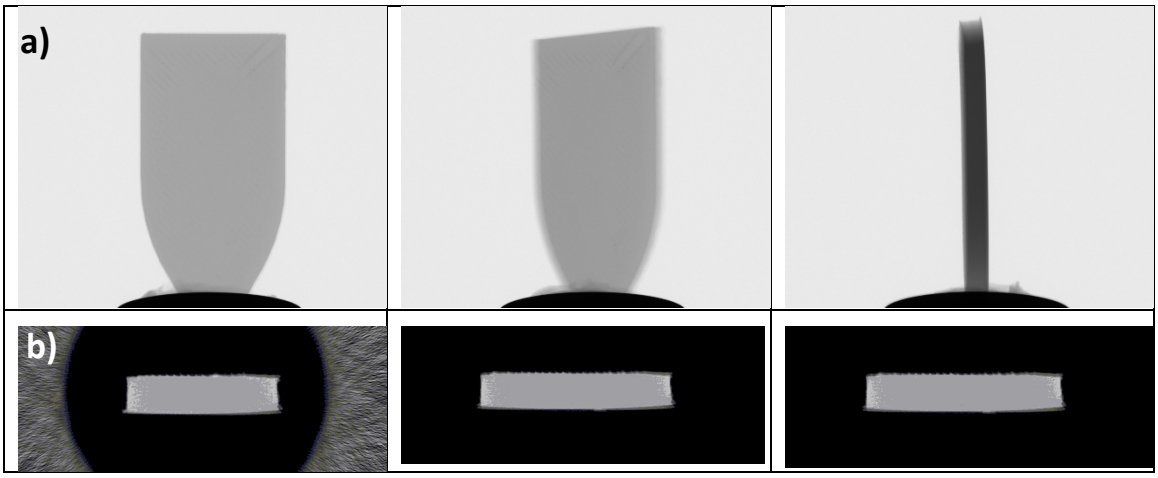

Figure 13. Micro-CT images of F0 (a) Binarized (1st Row) and (b) Reconstructed (2nd Row).

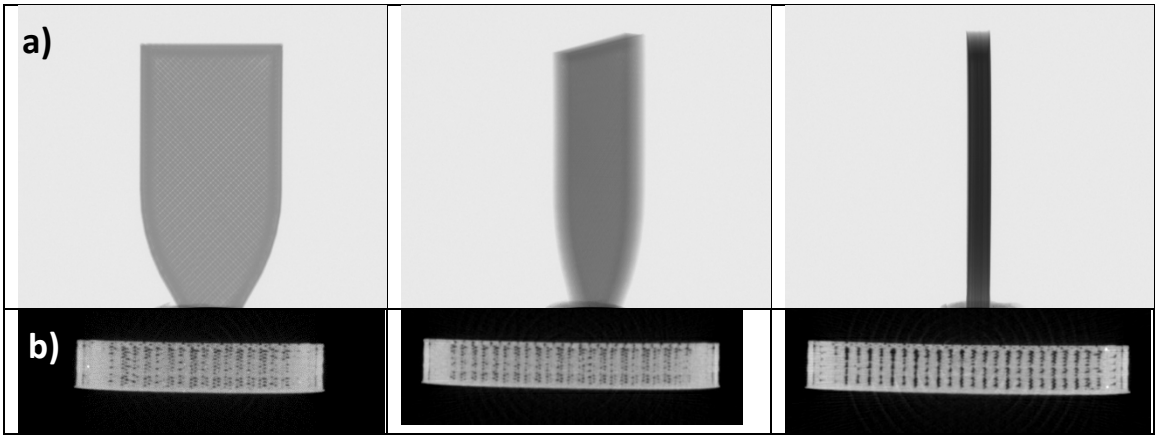

Figure 14. Micro-CT images of F5 (a) Binarized (1st Row) and (b) Reconstructed (2nd Row).

3. CONCLUSIONS

In this study, PA6/66 and its derivative formulations were successfully processed, printed, and characterized. After analysis of all tests, it was found from MCC that all formulations outperformed the neat PA6/66 system; among the results, F2, F4, and F5 yielded the best results. From TGA testing, all formulations outperformed the neat system. Furthermore, TGA displayed clear differences between the formulations containing 15 wt.% FR and 12.5 wt.% FR. UL 94 flammability testing also yielded promising results as F5 showed no drip formation, therefore, successfully 3D printing F2 and F4 may yield even better flammability properties. Although mechanical properties of F5 degraded in comparison to the neat system, it is believed that the other additives (NC, MWNT, and K) assisted in preventing the mechanical properties from deteriorating even further. Micro-CT analysis proved that F5 has much higher porosity in comparison to the control system, F0. This increase in porosity was most likely caused by the additives in the nanocomposite which decreased the material flow rate during the printing process.

4. FUTURE WORKS

Although SEM and TEM images are not taken yet, they are expected to show good dispersion of the additives. However, the SEM images will be closely observed to ensure that flame retardant is homogenously dispersed within the PA6/66 matrix because uneven dispersion of FR may have caused inconsistent UL 94 date. Furthermore, SEM can also be used to observe the surface morphology of the samples before and after UL 94 tests. Moving forward, more research will be conducted to adjust the 3D printing parameters to ensure successful prints with more PA6/66 formulations as well as printing test samples with lower porosity. Doing so will allow further UL 94 testing, tensile testing, and micro-CT analysis of more formulations.

Acknowledgments

This research was partially funded by KAI, LLC, Austin, Texas, USA. The authors acknowledge the facilities, and the technical assistance of the RMIT Advanced Manufacturing Precinct and RMMF Facility.

REFERENCES

[1] J. Koo, *Fundamentals, Properties, and Applications of Polymer Nanocomposites*, Cambridge University Press, Cambridge, UK, 2016, pp 389-424.

[2] H. Wu, M. Krifa, J.H. Koo, Rubber (SEBS-G-MA) Toughened Flame Retardant Polyamide 6: Microstructure, Combustion, Extension, and Izod Impact Behavior, *Polymer-Plastics Technology and Engineering* 57(8) (2017), 727-739.

[3] H. Wu, R. Ortiz and J. H. Koo, Self-Extinguishing and Non-Drip Flame Retardant Polyamide 6 Nanocomposite: Mechanical, Thermal, and Combustion Behavior, *Flame Retardancy and Thermal Stability of Materials* 1(1) (2018) 1-13.

[4] H. Wu, R. Ortiz, J.H. Koo, Rubber toughened flame retardant (FR) polyamide 11 nanocomposites Part 1: the effect of SEBS-g-MA elastomer and nanoclay, *Flame Retardancy and Thermal Stability of Materials* (2018), 1(1) (2018) 25-38.

[5] H. Wu, R. Ortiz, J.H. Koo, Rubber toughened flame retardant (FR) polyamide 11 nanocomposites Part 2: synergy between multi-walled carbon nanotube (MWNT) and MMT nanoclay, *Flame Retardancy and Thermal Stability of Materials* 2(1) (2018) 19-29.

[6] S.C. Lao, C. Wu, T.J. Moon, J.H. Koo, A. Morgan, L. Pilato, G. Wissler, Flame-Retardant Polyamide 11 and 12 Nanocomposites: Thermal and Flammability Properties, *Journal of Composite Materials* 43(17) (2009) 1803-1818.

[7] S.C. Lao, W. Yong, K. Nguyen, T.J. Moon, J.H. Koo, L. Pilato, G. Wissler, Flame-retardant Polyamide 11 and 12 Nanocomposites: Processing, Morphology, and Mechanical Properties, *Journal of Composite Materials* 44 (25) (2010) 2933-2951.

[8] S.C. Lao, J.H. Koo, T.J. Moon, M. Londa, C.C. Ibeh, G.E. Wissler, L.A. Pilato, Flame-retardant Polyamide 11 Nanocomposites: Further Thermal and Flammability Studies, *Journal of Fire Sciences* 29(6) (2011) 479-498.

[9] S.C. Lao, J.H. Koo, T.J. Moon, W. Yong, C. Lam, J. Zhou, B. Haisujoto, G. Wissler, L. Pilato, Z.P. Luo, Flame Retardant Intumescent Polyamide 11 Nanocomposites-Further Study, *Journal of Composite Materials* 47(923) (2013) 2973-2986.

[10] A. Hao, I. Wong, H. Wu, B. Lisco, B. Ong, A. Sallean, S. Butler, M. Londa, J.H. Koo, Mechanical, Thermal, and Flame-Retardant Performance of Polyamide 11-Halloysite Nanotube Nanocomposites, *Journal of Materials Science* 50 (1) (2015) 157-167.

[11] J.W. Gilman, T. Kashiwagi, J.D. Lichtenhan, Nanocomposites: a revolutionary new flame retardant approach, *SAMPE Journal* 33(4) (1997) 40-46.

[12] J.W. Gilman, Flammability and thermal stability studies of polymer layered-silicate (clay) nanocomposites, *Applied Clay Science* 15(1–2) (1999) 31-49.